

Highly accurate 9th-order schemes and their applications to DNS of thin shear layer instability*

A.I.Tolstykh , M.V.Lipavskii, E.N.Chigerev

Computing Center of Russian Academy of Sciences, Vavilova str.40, 119991 Moscow GSP-1,
Russia
tol@ccas.ru

1. Introduction

It is well known that high accuracy and high resolution methods are the most appropriate tools when numerically simulating small scale phenomena in fluid flows. In the case of finite difference schemes, the desired properties can be achieved by using high order approximations. Comparing with low-order schemes (say, with second-order ones), merits of high-order schemes come from larger domains of wave numbers supported by grids where phase and (possibly) amplitude errors are small. Comparing with low-order schemes (say, second order ones), considerably coarser meshes can be used with near minimum numbers of nodes falling into small scales subdomains to be properly resolved. To suppress spurious numerical solution oscillations, low-dissipative high-order schemes are preferable when dealing with high gradients solutions. Sometimes, some optimization is used to enlarge domains of small phase and amplitude errors [1]. However, another important issue seems to be how actually small are the errors in the physically relevant ranges of wave numbers supported by meshes. In this context, constructing as high order approximations as possible may be of importance. Following that strategy, we use our approach to create formally arbitrary order approximations to derivatives (or other grid functionals) without increasing numbers of nodes in stencils but increasing number of basis operators in their linear combinations ("multioperators"). The idea was first proposed in [2] and extensively used in our further investigations and computational practice. Some details of the technique can be found, for example, in [3], [4]. It can be especially efficient when using parallel machines. The scope of target problems includes (but is not limited to) DNS, LES, acoustics and other small scale phenomena. In the present paper, we consider its application to development of 2D thin shear layer instability with generating and decaying turbulence. Before doing so, we present brief outlines of a scheme with 9th order multioperators based approximations to convection terms.

2. Arbitrary order multioperators approximations

General formulations. For completeness, we present brief outlines of the multioperators principle. Suppose that there is a family of operators $L_h(s)$ dependent on, at least, one parameter s and approximating a linear operator L on a grid ω_h . Suppose further that for sufficiently smooth function $f \in U$ for each grid point with number j one has

$$[Lf]_j = L_h(s_i)[f]_j + \sum_{k=m}^{m+M-2} a_{kj}c_k(s_i)h^k + O(h^{m+M-1}) \quad (1)$$

where h is some parameter characterizing mesh size, a_{kj} are independent of h coefficients and $[\cdot]_h : U \rightarrow U_h(\omega_h)$ is a projection operator into a space U_h of grid functions defined on ω_h .

*This work was supported by the Russian Foundation for Basic Research (project no. 05-01-00584) and by basic-research program no. 3 of the Department of Mathematical Sciences, Russian Academy of Sciences (project no. 3.15).

The coefficients a_{kj} may be considered as high derivatives values at x_j . Assume also that the determinant

$$\det A \neq 0 \quad (2)$$

where $A = \{a_{ij}\}$, $a_{1j} = 1$, $a_{ij} = c_{m+i-2}(s_j)$ $i = 2, 3, \dots, M$, $j = 1, 2, \dots, M$ for all M . Then it is possible to find coefficients γ_i , $i = 1, 2, \dots, M$ such that (1) reduces to $[Lf]_j = \sum_{i=1}^M \gamma_i L_h(s_i)[f]_j + O(h^{m+M-1})$ for arbitrary M . The linear combination $L_M = \sum_{i=1}^M \gamma_i L_h(s_i)$ was named in [2] as multioperator while $L_h(s_i)$, $i = 1, 2, \dots, M$ may be viewed as basis operators. It is worth noting that the action of L_M on a known grid functions can be calculated in a parallel manner using at least M processors, each processor being involved in the synchronous calculations of the basis operators actions. Thus $m+M-1$ order can be achieved without adding complexity to approximating formulas, the corresponding execution times being independent of M when neglecting data transfer exchange.

The expression $L_h(s_i)[f]_j$ may be viewed as an approximation to any grid functional generated by a linear operator L (for example, quadratures, interpolation formulas etc.) but it is not necessary satisfy (2). It turned out that the one-parametric families of Compact Upwind Differencing operators (CUD) from [5] fit neatly into a class of $L_h(s_i)$ serving as basis operators. They are rational functions of three-point operators providing third- and fifth- order differencing formulas, parameter s defining either upwind or downwind discretizations of convection terms. Clearly, high orders of multioperators are not sufficient property when constructing numerical methods. Thus each multioperator needs individual treatment to meet some desirable properties (for example, upwinding in the case of fluid dynamics). Initially, third-order CUD were used as basis operators to create fifth- and seventh- order upwind schemes for fluid dynamics [6]. Later, multioperators based on centered compact approximations (not necessary to derivatives) with artificially introduced parameters were proposed [4]. Recently, a novel one-parametric family of non-centered compact approximations with two diagonal inversions and related multioperators were described [7]. Skipping the details, we concentrate on the scheme with a version of ninth-order approximation to the convection terms of the Navier-Stokes equations used in the thin shear layers calculations.

Multioperators based on fifth-order CUD. Introducing uniform mesh $\omega_h = \{x_j = jh, h = \text{const}, j = 0, \pm 1, \pm 2, \dots\}$ and three-point operators $\Delta(s) = (\Delta_0 - s\Delta_2)/2$, $\Delta_0 u_j = u_{j+1} - u_{j-1}$, $\Delta_2 u_j = u_{j+1} - 2u_j + u_{j-1}$, we consider the following fifth-order CUD operator from [5] as a generator of multioperators

$$L_5(s, \sigma) = \frac{1}{h} \left[\Delta(\sigma) + \frac{\sigma}{2} R^{-1}(s, \sigma) Q(s, \sigma) \left(E + \frac{1}{12} \Delta_2 \right)^{-1} \Delta_2 \right], \quad (3)$$

where s and σ are parameters satisfying $\text{sgn } s = \text{sgn } \sigma$, $|\sigma| = 2/\sqrt{5}$,

$$Q(s, \sigma) = E + (-1/15\sigma - s/4) \Delta_0 + (1/6 + s/15\sigma) \Delta_2,$$

$$R(s, \sigma) = E + (1/10\sigma - s/4) \Delta_0 + (1/6 - s/10\sigma) \Delta_2,$$

Considering the Hilbert space of grid functions defined on ω_h with the inner product $(u_h, v_h) = h \sum_{j=-\infty}^{\infty} u_j v_j$, L_5 is positive (negative) if $s > 0$ ($s < 0$) [5]. Moreover, $L_5(s)^* = -L_5(-s)$ thus providing upwinding when dealing with convection terms.

The Taylor expansion series for its action on a sufficiently smooth functions $u(x)$ looks as

$$L_5[u]_j = (u_x)_j + \left[\frac{h^5}{6!} p_1(s) u_x^{(6)} + \frac{h^6}{7!} p_2(s) u_x^{(7)} + \dots + \frac{h^8}{9!} p_4(s) u_x^{(9)} \right] + O(h^9) \quad (4)$$

where p_k – k th-order polynomials in s . For example, p_1, p_2, p_3 are given by

$$p_1 = -\frac{\sqrt{5}}{1800} - \frac{1}{144}s, \quad p_2 = \frac{53}{37800} + \frac{\sqrt{5}}{720}s - \frac{1}{288}s^2, \quad p_3 = -\frac{41\sqrt{5}}{216000} + \frac{1}{8640}s + \frac{\sqrt{5}}{1440}s^2 - \frac{1}{576}s^3$$

We fix five values of s to improve the conditioning of the resulting system we define them as zeroes of the Chebyshev fifth-order polynomial for the interval $[s_{min}, s_{max}]$: $0 < s_{min} = s_1 < \dots < s_5 = s_{max}$. Introducing the sum $L_{59} = \sum_{i=1}^5 \gamma_i L_5(s_i)$, $\sum_{i=1}^5 \gamma_i = 1$, and requiring that the coefficients for h^k , $k = 5, 6, 7, 8$ are equal to zero, we obtain the following linear system for γ_i , ($i = 1, \dots, 5$) with the known RHS r_j , $j = 1, 2, 3, 4$

$$\begin{bmatrix} 1 & 1 & \dots & 1 \\ s_1 & s_2 & \dots & s_5 \\ \dots & \dots & \dots & \dots \\ s_1^4 & s_2^4 & \dots & s_5^4 \end{bmatrix} \begin{bmatrix} \gamma_1 \\ \gamma_2 \\ \dots \\ \gamma_5 \end{bmatrix} = \begin{bmatrix} 1 \\ r_1 \\ \dots \\ r_4 \end{bmatrix} \quad (5)$$

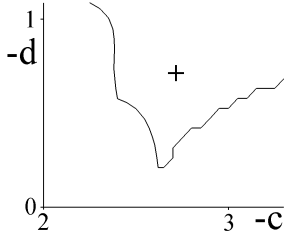


Figure 1.

Its solution gives $L_{59}(s_{min}, s_{max})[u]_j = [u_x]_j + O(h^9)$. It can be shown that $L_{59}(s_{min}, s_{max})^* = -L_{59}(-s_{min}, -s_{max})$. To organize upwinding, all we need is to find a pair (s_{min}, s_{max}) providing $L_{59}(s_{min}, s_{max}) > 0$. This can be accomplished by calculating the real part of \hat{L}_{59} , the Fourier transform of L_{59} , as a function of the Fourier variable kh where k is the wave number and the required pair. The pair for which $\Re \hat{L}_{59} > 0$ can be viewed as an admissible one. The calculations showed that the positivity region corresponds to negative values of s_{min}, s_{max} . It is marked with "+" in Fig. 1

where parameters d and c are defined by $s_{max} + s_{min} = 2c$, $s_{max} - s_{min} = 2d$. The spectral properties of L_{59} can be illustrated by using the simple IVP for advection equation

$$\partial u / \partial t + a \partial u / \partial x = 0, \quad u(x, 0) = \exp(ikx) \quad (6)$$

in which $(\partial u / \partial x)_j$ is discretized by L_{59} . Considering $\exp(ikx_n)$, $n = \pm 1, \pm 2, \dots$, as the eigen function of L_{59} in the space of bounded grid functions with the norm $\|u_h\| = \max |u_i|$, $i = 0, \pm 1, \pm 2, \dots$ and defining the eigenvalues as a function of $\alpha = kh$ where k is the nondimensional wave number by $L_{59} e^{i\alpha n} = (p(\alpha) + iq(\alpha)) e^{i\alpha n}$, $n = 0, \mp 1, \mp 2, \dots$; $0 \leq \alpha \leq 2\pi$

$$u_j(t) = e^{-ap} e^{ik(x_j - a_* t)} \quad (7)$$

where a_* is the "numerical" phase velocity given by $a_* = aq(\alpha)/\alpha$. The exact solution of (6) can be obtained from (7) via substitution $p \rightarrow 0$ $a_* \rightarrow a$. The dissipation parameter p which is formally equal to $\Re \hat{L}_{59}$ should be positive in the case of a stable scheme.

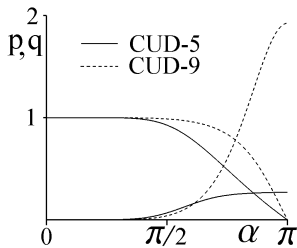


Figure 2.

Fig. 2 shows functions $p(\alpha)$ and $a_*/a = q(\alpha)$ for an admissible pair (dashed lines) compared with those in the case of L_5 operator for some s value (solid lines). They define the corresponding amplitude and phase errors. The errors are characterized by the deviations from 0 and 1 respectively. The curves of this type visually typical for all high-order schemes. They show that the errors are small at least for $\alpha = kh < \pi/2$ (that is, for the wave length $\Lambda > 4h$). However, their actual values in that range influencing accuracy of the harmonics representation essentially depend on approximation orders. The interval $\pi/2 \leq kh < \pi$ corresponds to the scales poorly resolved by

meshes with sizes h . As is evident from the graphs, considerable damping of the harmonics may be expected in that region. Thus the multioperator has high-order dissipative mechanism serving as a built-in filter of non-physical oscillations. It is worth noting that the admissible values of s_{min} and s_{max} can be used to control to some extent the dispersion and dissipation.

Application to fluid dynamics. We illustrate convection terms multioperators discretization using non-linear conservation law

$$\partial u / \partial t + \partial f(u) / \partial x = 0 \quad (8)$$

To construct semi-discretized schemes with positive spatial discretizations (in the "frozen coefficients" sense), we use the flux splitting

$$f(u) = f^+ + f^-, \quad f^+ = (f(u) + cu)/2, \quad f^- = (f(u) - cu)/2, \quad c = \text{const} > 0 \quad (9)$$

Supposing that s_{min}, s_{max} are chosen to define $L_{59} > 0$, we construct the following approximation

$$\partial f(u)/\partial x|_{x=x_j} = L_{59}f_j + O(h^9), \quad L_{59}f_j = L_{59}^+f^+|_{x=x_j} + L_{59}^-f^-|_{x=x_j},$$

$L_{59}^\pm = L_{59}(\mp s_{min}, \mp s_{max})$. It is easy to see that $L_{59}f > 0$ for $f(u) = au$, $a = \text{const}$.

Now the linearly stable semi-discretized scheme for (8) can be written as

$$\partial u/\partial t + L_{59}f = 0. \quad (10)$$

Fully discretized schemes for (8) can be obtained by specifying a time stepping procedure depending on a particular problem. For unsteady problems, the Runge-Kutta methodology can be used. Scheme (10) can be easily extended to multidimensional and/or vector-valued functions.

In all cases, they are conservative meaning that actions $L_{59}f_j$ can be presented as the difference of numerical fluxes $L_{59}f_j = q_{59,j+1/2} - q_{59,j-1/2}$, the last being obtained from the similar representation for $L_{59}f_j$ by summation with the γ coefficients.

Numerical example. To illustrate comparative accuracy of the above scheme, we consider the following popular test problem (see for example [1])

$$\partial u/\partial t + \partial(u^2/2)/\partial x = 0$$

with $u(0, x) = 1 + 0.5 \sin(\pi x)$ and periodic boundary condition $u(t, -1) = u(t, 1)$. The exact solution is smooth up to $t = 2/\pi$ and can be easily obtained via the iteration procedure described in [1]. It allows to calculate the numerical solution errors and the corresponding mesh convergence orders given by

$$E_c(n) = \max_{j=0, n-1} |u_j^{num} - u_j^{exact}|, \quad k_c = \log_2 E_c(n)/E_c(2n)$$

where n is the number of grid points. In the Table, the results of calculations with the fourth-order Runge-Kutta time stepping are presented for the schemes with L_5 , L_{59} and fifth-order WENO scheme [8].

n		8	16	32	64	128	256	512
WENO-5	E_c	6.47e-2	1.25e-2	1.20e-3	9.50e-5	3.31e-6	8.66e-8	2.25e-9
	k_c		2.37	3.38	3.66	4.84	5.26	5.27
L_5	E_c	3.99e-2	6.10e-3	4.35e-4	1.63e-5	5.11e-7	1.56e-8	4.83e-10
	k_c		2.71	3.81	4.74	5.00	5.03	5.01
L_{59}	E_c	3.30e-2	2.89e-3	1.30e-4	2.17e-6	1.30e-8	3.46e-11	7.51e-14
	k_c		3.51	4.47	5.91	7.38	8.55	8.85

As seen, the least accurate is the WENO scheme while the scheme with L_{59} shows dramatic increase of accuracy with increasing n . It should be noted that more refined mesh requires higher-precision arithmetics.

3. Application to shear layer instability.

Problem formulation. We consider the following double periodic problem for the incompressible Navier-Stokes equations. At an initial time moment $t = 0$, two thin shear layers are specified in the form of the Cartesian velocities components u and v given by

$$\begin{aligned} u &= \text{th} \left[\rho \left(y - \frac{1}{4} \right) \right] \text{ for } y \leq \frac{1}{2}, & u &= \text{th} \left[\rho \left(\frac{3}{4} - y \right) \right] \text{ for } y > \frac{1}{2}, \\ v &= \delta \sin(2\pi mx), \end{aligned}$$

where ρ and δ defines the layers thickness and the initial perturbation of the y -component respectively, m being a number of the perturbation harmonics.

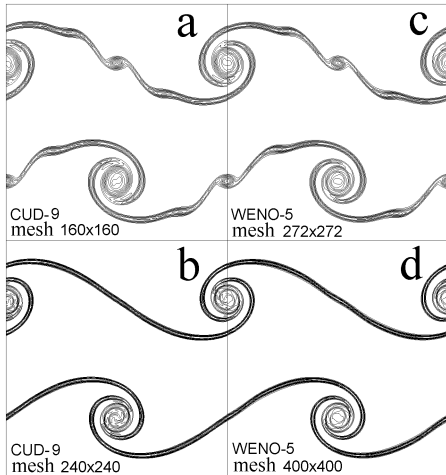


Figure 3.

The above formulation was considered in [9],[10] where various schemes were tried to simulate the time evolution of the layers. The calculations carried out for relatively small time interval ($t \leq 1.2$) revealed an interesting fact. It turned out that during the layers rolling up process a spurious vortices do appear even if sufficiently refined 256×256 mesh is used. The artifact disappeared in the case of 512×512 mesh. In [11], the same problem was used to test the fifth-order CUD scheme from [5]. It was found that the obtained solutions were visually the same as the above mentioned, the only difference being due to coarser 128×128 and 256×256 meshes used in the calculations. It is worth noting that our recent calculations with the WENO-5 scheme showed that the artifact still exists when using 272×272 meshes.

The occurrence and disappearing of the spurious vortices is illustrated in Fig. 3a,b,c,d. Fig 3a,b and 3c,d correspond to our ninth-order CUD-9 and WENO-5 calculations.

The results presented in [9], [10] and [11] concerned with small time intervals. Below we present the complete history of the flow field time evolution with true resolution of all spatial scales. The smallest ones correspond to 2D turbulent pulsations requiring according to the general theory $O(Re)$ degrees of freedom for their simulation. To perform such type of calculations for large time intervals, schemes with very small phase and amplitude errors are needed.

Schemes outlines. The simulations were carried out using the Navier-Stokes equations written for the vorticity ω and the stream function ψ . The conservative form of the inviscid terms of the vorticity transport equation were approximated with the above described methodology using either L_5 or L_{59} operators. To discretize the second derivatives in the Poisson equation for ψ and the ψ derivatives needed to calculate the velocities, the sixth-order centered compact formulas were used. It was found that very small truncation errors of the centered compact approximation do not noticeably influence the obtained numerical solutions. The time stepping was performed with the fourth-order Runge-Kutta procedure using as small time step as needed to exclude its impact on the solutions. The calculations were carried out for the Reynolds number $Re = 4 \cdot 10^4$, $Re = 10^5$, $Re = 4 \cdot 10^5$, $Re = \infty$ and meshes 512×512 , 1024×1024 2048×2048 . For all Re numbers, the mesh convergence was seen with complete resolution of the smallest scales. As an illustration

General view of the flow evolution. The calculations carried out for the Reynolds number $Re = 4 \cdot 10^4$, $Re = 10^5$, $Re = 4 \cdot 10^5$, $Re = \infty$ and meshes 512×512 , 1024×1024 2048×2048 . The general scenario given by the numerical solutions for the main perturbation harmonics ($m = 1$) in the terms of vorticity contours looks as follows. As

a result of a small perturbation of the velocity v introduced at $t = 0$ and then removed, the shear layers rolling up occurs with forming concentrated vorticity regions connected

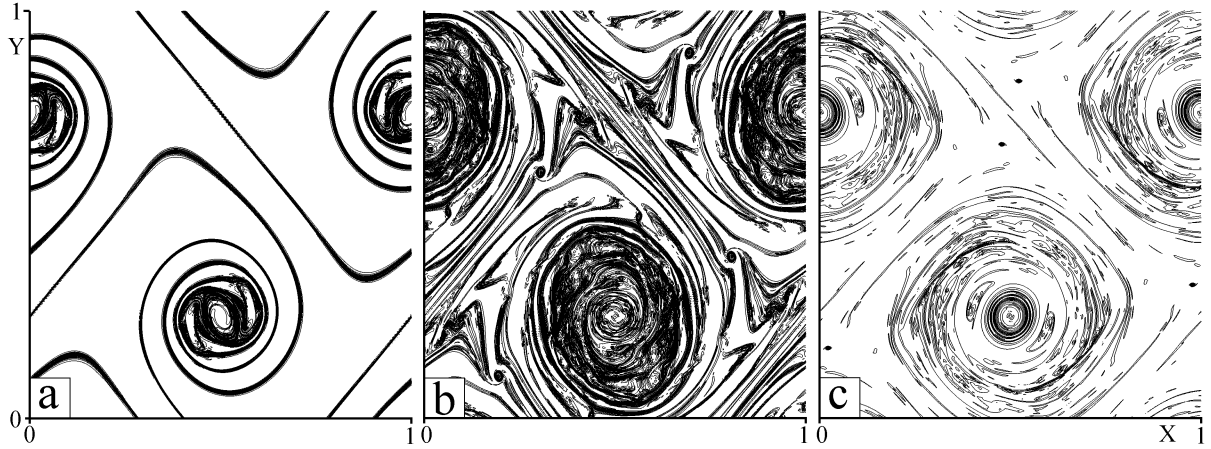


Figure 4.

with thin links (Fig. 4a). The links thereafter disrupts and the vorticity regions are shaped into isolated vortices (Fig.4b). The ensuing flow development is characterized by forming thin vorticity fibres emanating from the main vortices. The fibres can be viewed in turn as shear layers degenerating into small vortices. The last dissipate but new small vortices appear from subsequent emanated fibres. At the latest stages isolated vortices with opposite signs separated by visually vorticity-free regions are seen (Fig. 4c). The vortices cores are characterizes by decaying small scales structures.

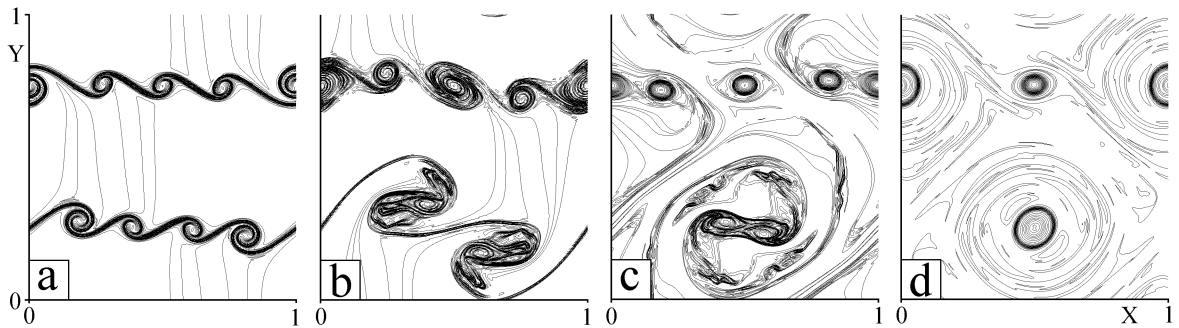


Figure 5.

In the case of a combination of the main harmonic and subharmonics ($m > 1$), the scenario looks like the above described, the only differences being due to the vortices pairing resulting in a non-symmetric their final arrangement. The general view of the vorticity field evolution is show in Fig. 5a,b,c,d.

For all considered Re numbers, the mesh convergence was seen with complete resolution of the smallest scales. As an illustration, the vortex cross-section $t =$ with its fine details is shown in Fig. 6. ($m = 2, t = 2.2$). The peaks seen in the Figure are the cross sections of the emanating fibres.

In the case $Re = \infty$, the vorticity field evolution looks like that for $Re = 400000$. However there were no mesh convergence since more refined meshes generated finer small scale vortex structures.

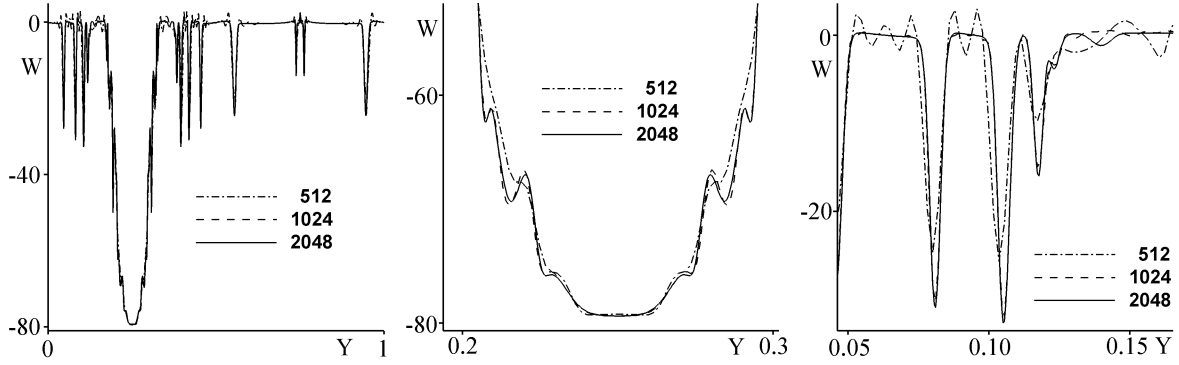


Figure 6.

Turbulence spectra. Due to the shear layers instability, turbulent fluctuations are generated at some time moment and then freely decays due to lack of the energy injection. An analysis of the energy and the enstrophy spectra at successive time moments clearly indicates their cascade to higher wave numbers. The energy spectra at time $t = 2.2$ corresponding to the main perturbation ($m = 1$) and that with the subharmonics $m = 2, 3, 4$ are shown in Fig.7 with the theoretical k^{-3} curve, the wave number k being normalized using the computational domain length $L = 1$. As seen, the difference between curves corresponds to the large eddies wave numbers while in the highest wave number range they show closely related behavior.

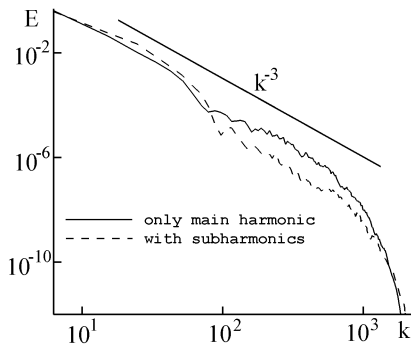


Figure 7.

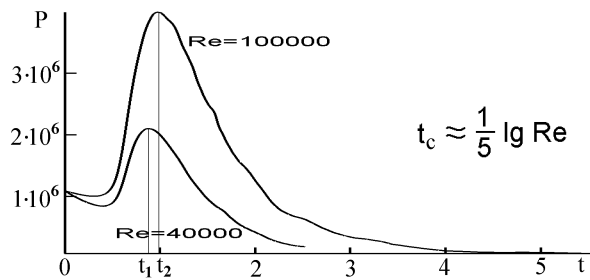


Figure 8.

In [12], the estimate for the "critical" time t_c for which the so called palinstrophy $P(t)$ which characterize the *rot* of *rot* reaches its maximum is presented. It indicates that it is approximately proportional to the Reynolds number. In Fig.8, the function is shown for $Re = 40000$ and $Re = 100000$. The obtained t_c agrees excellently with the estimate.

References

- [1] N. A. Adams, K. Sharif, "A high-resolution compact-ENO scheme for shock-turbulence interaction problems", *J. Comput. Phys.*, **127**, 27–51 (1996).
- [2] A. I. Tolstykh, "Multioperator high-order compact upwind methods for CFD parallel calculations", in *Parallel Computational Fluid Dynamics*, Elsevier, Amsterdam, 383–390 (1998).
- [3] A. I. Tolstykh, "On multioperators principle for constructing arbitrary-order difference schemes", *Applied Numerical Mathematics*, **46**, 411–423 (2003).

- [4] A. I. Tolstykh, “Centered prescribed-order approximations with structured grids and resulting finite-volume schemes”, *Applied Numerical Mathematics*, **49**, 431–440 (2004).
- [5] A. I. Tolstykh, “High accuracy non-centered compact difference schemes for fluid dynamics applications”, *World Scientific*, Singapore, (1994).
- [6] M. V. Lipavskii and A. I. Tolstykh, “Fifth- and Seventh-Order Accurate Multioperator Compact Schemes”, *Computational Mathematics and Mathematical Physics*, **43**, no. 7, 975–990 (2003).
- [7] A. I. Tolstykh, “A Family of Compact Approximations and Related Multioperator Approximations of a Given Order”, *Doklady Mathematics*, **72**, no. 1, 519–524 (2005).
- [8] X.-D. Liu, S. Osher and T. Chan, “Weighted essentially non-oscillatory schemes”, *J. Comput. Phys.*, **115**, 200–212 (1994).
- [9] D. L. Brown and M. L. Minion, “Performance of under-resorved two-dimensional incompressible flow simulations”, *J. Comput. Phys.*, **122**, 165–183 (1995).
- [10] M. L. Minion and D. L. Brown, “Performance of under-resorved two-dimensional incompressible flow simulations, II” *J. Comput. Phys.*, **138**, 734–765 (1997).
- [11] A. I. Tolstykh and E. N. Chigirev, “On thin shear layers numerical simulation”, *J. Comput. Phys.*, **166**, 152–158 (2001).
- [12] M. Lesieur “Turbulence in Fluids”, *Kluwer*, Dordrecht, (1990).